Scalar Mixing Modeling in PDF Simulations of Turbulent Premixed Flames

Michael K. Stoellinger and Stefan Heinz

Department of Mathematics, University of Wyoming
1000 East University Avenue, Laramie, WY 82071, USA

Email:*mstoell@uwyo.edu*

ABSTRACT

The use of probability density function (PDF) methods for turbulent combustion simulations is very attractive because arbitrary finite-rate chemistry can be exactly taken into account. However, many real flames involve a variety of mixing regimes, and the development of PDF methods for partially-premixed and premixed turbulent combustion turned out to be a very challenging task. The paper shows a promising way to overcome this problem by extending existing PDF methods such that a variety of mixing regimes can be covered. The latter is done by a generalization of the standard scalar mixing frequency model. The suitability of the new mixing frequency model is shown by applications to several premixed turbulent Bunsen flames which cover various regimes ranging from flamelet to distributed combustion.

1. INTRODUCTION

The extension of Reynolds-averaged Navier-Stokes (RANS) equations by probability density function (PDF) methods [1, 2] has significant advantages for turbulent reacting flow simulations due to the fact that there is no need to involve approximations of uncertain generality to close chemical reaction rates. Due to the exact treatment of chemical reactions, the performance of PDF methods is essentially determined by the modeling of the transport of scalars. Such scalar transport models involve two ingredients: a scalar mixing frequency model that determines the characteristic time scale of mixing, and a scalar mixing model that describes the change of the PDF of a scalar [2].

Most of the previous applications of PDF methods were related to simulations of non-premixed turbulent combustion. In this case, the characteristic length and time scales of scalar fields are usually larger than the characteristic length and time scales of turbulent motions. Correspondingly, the scalar mixing frequency can be assumed to be controlled by the frequency of large-scale turbulent motions. Applications of PDF methods to premixed turbulent combustion are more complicated than calculations of non-premixed turbulent combustion. The appearance of fast flamelet chemistry may result in very thin reaction zones such that scalar mixing can take place on scales which are much smaller than all scales of turbulent motions [3, 4]. Correspondingly, there exist only a few applications of PDF methods to premixed flames. To overcome problems of earlier approaches, Mura et al. [4] recently suggested a PDF model where the outer parts of the flame structure (reactant side and product side) are described by a standard scalar mixing model whereas the inner part (the reaction zone) is described by a flamelet model. However, this approach is complicated and related to several questions (e.g. regarding the matching of both combustion regimes). More recently, Lindstedt and Vaos [5] developed a model that relates the scalar mixing frequency of reacting scalars to the characteristic frequency of turbulent motions and the scalar mixing frequency of non-reacting scalars, respectively. However, the approach uses several assumptions which are not satisfied in general [6].

To address the problems of PDF methods described above, we present a new model for the scalar mixing frequency. The model is constructed such that deviations from a local equilibrium between production processes and dissipation of scalar variance are mini-

mized. Details on the model derivation and characteristic features can be found elsewhere [6]. The performance of the new model will be demonstrated by applications to three turbulent premixed Bunsen flames.

2. THE MODELING APPROACH

The evolution of the scalar PDF $F_\theta(\boldsymbol{\theta};\boldsymbol{x},t)$ is governed by the transport equation [1, 2]

$$\frac{\partial \langle\rho\rangle F_\theta}{\partial t}+\frac{\partial \langle\rho\rangle \overline{u}_i F_\theta}{\partial x_i}=\frac{\partial}{\partial x_i}\langle\rho\rangle\ \frac{\overline{\nu}+\nu_t}{Sc_t}\frac{\partial F_\theta}{\partial x_i} - \sum_{\alpha=1}^{N_s}\frac{\partial}{\partial \theta_\alpha}\langle\rho\rangle\left(M_\alpha^{''}+S_\alpha\right)F_\theta. \quad (1)$$

Here, the conditional turbulent scalar flux is parametrized by the gradient diffusion assumption [1, 2].

The scalar PDF transport equation (1) is unclosed as long as the molecular mixing term $M_\alpha^{''}$ is not specified. The latter can be done in a variety of ways [1, 2]. We will use a parametrization of $M_\alpha^{''}$ according to the interaction-by-exchange-with-the-mean (IEM) mixing model [7],

$$M_\alpha^{''}=-\frac{C_\alpha}{2\tau}\phi_\alpha^{''}. \quad (2)$$

The model (2) represents the standard mixing model which is used in most simulations of turbulent reacting flows [2]. The reason for that is given by the simplicity of the model (2). The model (2) contains two ingredients: a scalar mixing model that describes changes of scalar values, and a scalar mixing frequency model that determines the characteristic time scale of mixing. The scalar mixing is modeled by $-\phi_\alpha^{''}$, which corresponds to the idea that scalar fluctuations $\phi_\alpha^{''}$ tend to disappear (scalar values ϕ_α tend to relax to their mean value $\overline{\phi}_\alpha$). The scalar mixing frequency $\omega_\alpha=C_\alpha/(2\tau)$ is modeled in proportionality to the mixing frequency $1/\tau$ of large-scale turbulent motions, where C_α is a nondimensional parameter. The consideration of the relatively simple standard mixing model (2) represents a natural first step of investigations of the performance of improved models for the mixing frequency ω_α in $M_\alpha^{''}$ models. Expression (2) requires the definition of C_α in order to specify the scalar mixing frequency $\omega_\alpha=C_\alpha/(2\tau)$. Mura et al. [4] showed that the standard value $C_\alpha=2$ is not applicable to premixed turbulent combustion. The scalar mixing frequency ω_α determines, first of all, the evolution of the scalar variance. Thus, the equation for scalar variances represents the natural basis for the definition of C_α. By adopting expression (2), the PDF transport equation (1) implies for scalar variances the transport equation [6]

$$E_\alpha=A_\alpha-C_\alpha B_\alpha. \quad (3)$$

B_α is given by $B_\alpha=\overline{\phi_\alpha^{''2}}/\tau$, and E_α and A_α are given by the expressions

$$E_\alpha=\frac{\bar{D}\overline{\phi_\alpha^{''2}}}{\bar{D}t}-\frac{1}{\langle\rho\rangle Sc_t}\frac{\partial\langle\rho\rangle(\overline{\nu}+\nu_t)}{\partial x_k}\frac{\partial\overline{\phi_\alpha^{''2}}}{\partial x_k}, \quad (4)$$

$$\begin{aligned}A_\alpha &= 2\frac{\overline{\nu}+\nu_t}{Sc_t}\left(\frac{\partial\overline{\phi}_\alpha}{\partial x_k}\frac{\partial\overline{\phi}_\alpha}{\partial x_k}+\frac{1}{2}\frac{\partial^2\overline{\phi_\alpha^{''2}}}{\partial x_k^2}\right)\\ &+ 2\overline{S_\alpha^{''}\phi_\alpha^{''}}. \end{aligned} \quad (5)$$

Here, $\bar{D}/\bar{D}t=\partial/\partial t+\overline{u}_k\,\partial/\partial x_k$ refers to the mean Lagrangian time derivative. It is worth noting that equation (3) represents an exact rewriting of the scalar variance equation. The notion of representing the scalar variance equation in terms of relation (3) is to combine the relevant processes on the right-hand side. The term E_α then represents deviations from the local equilibrium between production processes and dissipation. Equation (3) represents the basis for the calculation of C_α. The calculation of E_α, A_α, and B_α by simulation data results in fluctuating variables E_α, A_α, and B_α due to the effects of the discretization of equations and the finite number of particles involved in the Monte Carlo simulation. Therefore, C_α will be chosen such that the averaged quadratic error $\langle E_\alpha^2\rangle_T$ will become minimal. Here, $\langle Q\rangle_T$ refers to the temporal average of any variable Q. By analyzing $\langle E_\alpha^2\rangle_T$ as a function of C_α one finds that

$$C_\alpha=\frac{\langle A_\alpha B_\alpha\rangle_T}{\langle B_\alpha^2\rangle_T} \quad (6)$$

minimizes the averaged quadratic error $\langle E_\alpha^2\rangle_T$. The difference between the standard model assuming a constant value for C_α and the C_α model (6) is given by the fact that the model (6) provides local C_α values which minimize the deviations from the local equilibrium between production processes and dissipation of scalar variances. In addition to velocity-scalar correlations, the model (6) also accounts for velocity-variance correlations (given by the second term in the parentheses expression of (5)) and scalar-reaction correlations (given by the $2\overline{S_\alpha^{''}\phi_\alpha^{''}}$ term in (5)). Thus, the model (6) will be referred to below as generalized correlation (GC) model. The performance of this modeling concept in simulations will be discussed in the following sections in comparison to other C_α models.

3. THE FLAMES CONSIDERED

The turbulent premixed F1, F2, and F3 flames studied experimentally by Chen et al. [8] are considered to study the performance of the PDF modeling approach. The three highly stretched stoichiometric methane-air flames cover a range of Reynolds and Damköhler numbers. Based on an order of magnitude analysis Chen et al. [8] found that all three flames are located in the distributed reaction zones regime. In particular, the F1 flame is located at the borderline to the well stirred reactor regime, and the F3 flame is located at the borderline to the flamelet regime. Due to the simple configuration, the broad range of combustion conditions, and the high quality experimental database, the flames considered are well appropriate to study the performance of PDF methods for premixed turbulent combustion.

The three flames are generated with the same burner. The burner design is shown schematically in figure 1. The burner consists of a nozzle with diameter $D = 12mm$ for the main stream which is surrounded by a large pilot stream to stabilize the turbulent main jet flame. The laminar pilot stream is generated by an array (1165 holes of diameter 1 mm) of small jets issued through a cooled perforated plate. Both streams have a stoichiometric methane-air mixture (equivalence ratio $\Phi = 1$). The burner is surrounded by air at rest. The outer air is entrained into the three flames at axial positions 3D-5D, changing the flame brush to non-perfectly premixed.

The experimental database includes radial profiles of the mean velocity, the turbulent kinetic energy, mean and variance of the temperature, and the mean mass fractions of the major species CH_4, O_2, CO_2, H_2O and minor species CO, H_2, OH. The error in the measurements of the mean velocity is estimated to be less than 1%, and the error of the mean temperature is expected to be less than 10%. The error in the measurements of the major species is between 8% to 15%, and the error regarding the minor species is within 20% to 25%.

4. FLAME SIMULATIONS

A hybrid PDF-RANS approach was used to simulate the turbulent premixed flames described in section 3. Steady-state RANS equations were used for the calculation of the velocity field. The realizable $k - \varepsilon$ turbulence model of Shih et al. [9] was applied to provide the turbulent kinetic energy and characteristic frequency $1/\tau$ of large-scale turbulent motions. The

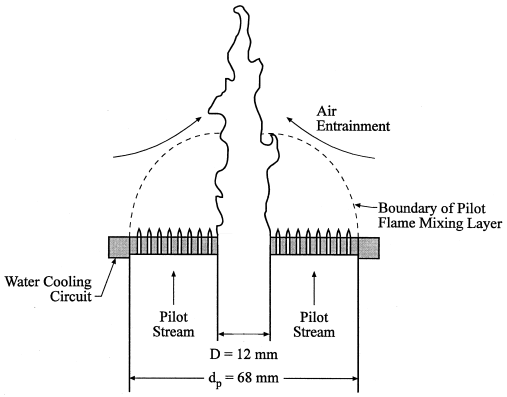

Figure 1: The burner design.

scalar PDF transport equation (1) was closed with the mixing model (2) combined with the model (6) for C_α. The PDF transport equation (1) was solved by Monte Carlo simulation. C_α was calculated according to the GC model (6) for the fuel (CH_4) mass fraction because combustion takes place only if fuel is available. A numerical limit $\overline{\phi_\alpha''^2} \geq 10^{-6}$ was applied to avoid the calculation of unphysically high values for C_α in regions where the scalar variance $\overline{\phi_\alpha''^2}$ becomes very small. Temporally averaged variables involved in the calculation of C_α according to relation (6) were obtained by a moving average over 50 iterations.

The steady-state RANS equations were discretized by the finite volume method. The particle equations are solved numerically by a mid-point rule [10] in order to achieve second order accuracy in time. The time step is determined from a local time stepping procedure. The number of particles per cell is set to 50. A higher number of particles per cell was found to have no effect on simulation results. The statistical error is further reduced by averaging over the last 200 iterations. All computations presented have been performed by using the FLUENT code [11].

The chemical reaction rates $S_\alpha(\boldsymbol{\phi})$ were provided by a skeletal chemical mechanism DRM22 [12] consisting of 23 species (H_2, H, O, O_2, OH, H_2O, HO_2, H_2O_2, CH_2, $CH_2(S)$, CH_3, CH_4, CO, CO_2, HCO, CH_2O, CH_3O, C_2H_2, C_2H_3, C_2H_4, C_2H_5, C_2H_6, N_2) and 104 elemental reaction. The composition change due to chemical reactions was treated by the *in situ* adaptive tabulation (ISAT) method developed by Pope [13].

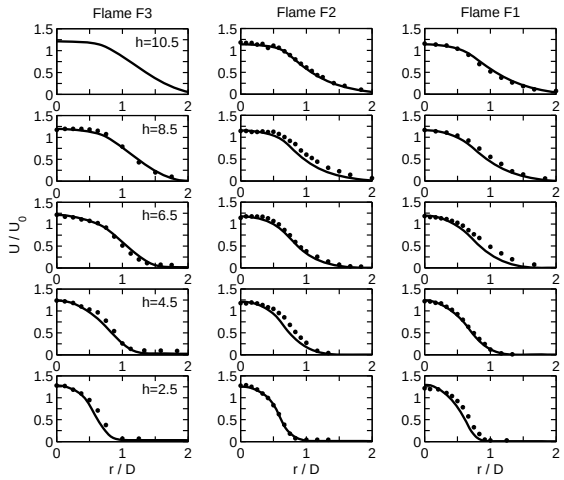

Figure 2: Normalized mean axial velocities U/U_0 for the F3, F2, and F1 flames. Dots denote experimental results of [8], and lines denote simulation results.

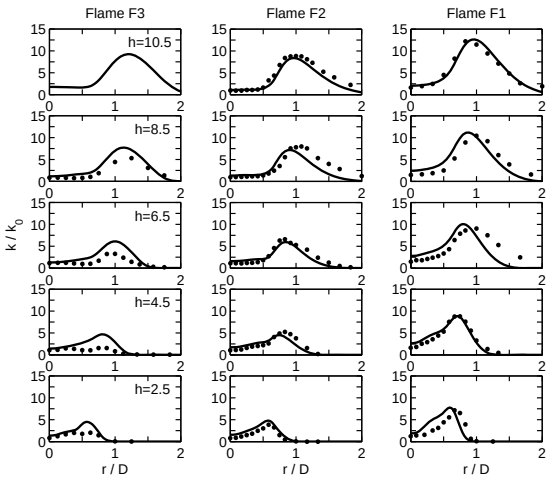

Figure 3: Normalized turbulent kinetic energy k/k_0 for the F3, F2, and F1 flames. Dots denote experimental results of [8], and lines denote simulation results.

The equations were solved on a 2-dimensional axisymmetric domain. The domain extends up to $20D$ downstream (axial direction) from the nozzle exit plane and $6.5D$ in radial direction to allow entrainment of the ambient air. Here, D refers to the nozzle diameter. The domain is discretized into 220×70 (axial by radial) cells. The grid is non-uniform to improve the accuracy of computations in the flame region. The grid independence of the solution has been checked by comparison with results obtained on a 260×100 grid. The profiles for the axial velocity and turbulent kinetic energy at the jet inlet have been taken from the experimental database of Chen et al. [8]. The profile for the turbulent dissipation rate has been calculated from the profile of the turbulent kinetic energy and measurements of the lateral length scale l_{lat} by adopting the relation $\varepsilon = (2k/3)^{3/2}/l_{lat}$ [8]. The pilot composition was calculated from the chemical equilibrium of a stoichiometric methane-air mixture with 20% heat loss.

5. SIMULATION RESULTS

Radial profiles of the normalized mean axial velocity U/U_0 are presented in figure 2 at different axial positions $h = x/D$. The mean axial velocity $U = \overline{u}_1$ is normalized by the bulk velocity $U_0 = 30, 50, 65\, m/s$ for the F3, F2, and F1 flames, respectively. The overall agreement between simulation results and measurements is excellent. The thermal expansion within the turbulent jet can be recognized by the increase of the axial velocity at radial positions $r/D > 0.5$ along the x-axis for all three flames. As a result of this expansion, the shear layer (which is roughly located at the position of the maximum gradient of the mean axial velocity) is pushed outward in radial direction. This trend can also be seen in figure 3 where radial profiles of the normalized turbulent kinetic energy k/k_0 ($k_0 = 3.82, 10.8, 12.7\, m^2/s^2$ for the F3, F2, and F1 flames, respectively) are shown. The peaks of the turbulent kinetic energy k are shifted outward for increasing axial positions. The results for the higher Reynolds number F2 and F1 flames agree very well with the measurements whereas an overprediction of the turbulent kinetic energy can be seen regarding the F3 flame, especially close to the burner head. Similar overpredictions have been reported by Lindstedt and Vaos [5]. The F3 flame was also studied by Pitsch and De Lageneste [14] by using large-eddy simulation (LES) in combination with a level set approach. Their turbulent kinetic energy results show a better agreement at $h = 2.5$ but a similar disagreement at $h = 6.5$. The F3 flame has the lowest axial velocity and the highest temperature. Thus, low Reynolds number effects which are not accounted for in the $k-\varepsilon$ model applied may be the reason for the turbulent kinetic energy overprediction.

Figure 4 shows radial profiles of the mean reaction progress variable $C = (\overline{T} - T_u)/(T_b - T_u)$ at different axial positions for the three flames considered. Here, $\overline{T}$ is the mean temperature, $T_b = 2248\, K$ is the adiabatic flame temperature and $T_u = 298\, K$ is the

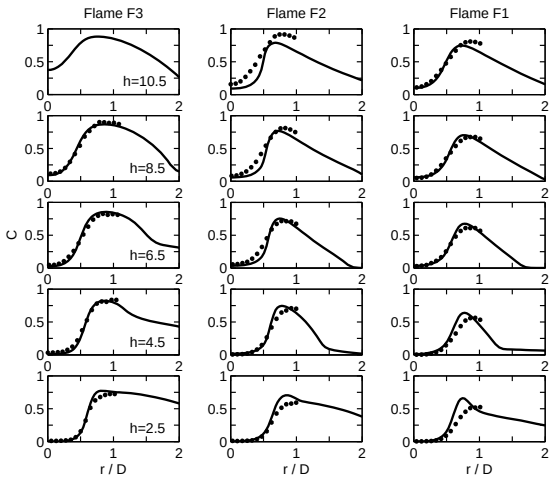

Figure 4: Mean reaction progress variable C for the F3, F2, and F1 flames. Dots denote experimental results of [8], and lines denote simulation results.

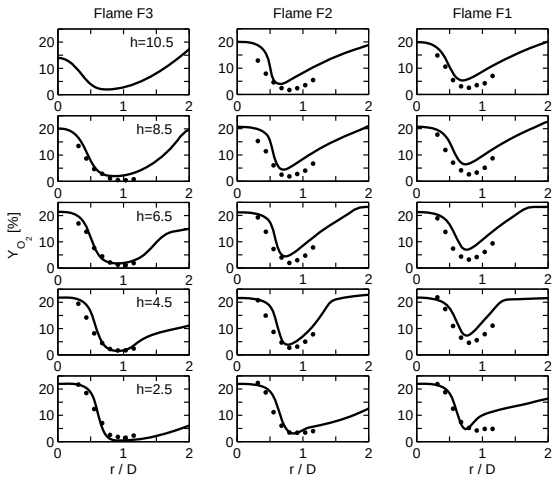

Figure 5: Mean O_2 mass fraction Y_{O_2} in percent for the F3, F2, and F1 flames. Dots denote experimental results of [8], and lines denote simulation results.

temperature of the surrounding air. The simulation results of the F3 flame agree very well with the measurements. This agreement indicates that the new GC frequency model is well applicable to flamelet conditions. The F2 and F1 flame simulation results show an overprediction of the progress variable at $h = 2.5$. Lindstedt and Vaos [5] found a similar overprediction in their F1 flame simulations using the same pilot inlet conditions. A reason for the observed overprediction of the temperature close to the burner exit regarding the F2 and F1 flames could be given by the complex interaction between the turbulent jet and laminar pilot stream. Such flow conditions are rather difficult to predict within the RANS framework. LES results for the F2 and F1 flames could clarify whether this is indeed the reason for the observed overprediction. However, such LES results have not been reported so far. Possibly, a better agreement between simulation results and measurements may be obtained by adopting refined inlet conditions (e.g., a reduction of the pilot inlet temperature regarding the F2 and F1 flames).

Figure 5 shows simulation results of the mean oxygen mass fraction Y_{O_2}. The oxygen concentration is well predicted in all three flames. The entrainment of surrounding air is clearly visible in figure 5. It is most intense in the highest Reynolds number F1 flame due to the high turbulence intensity.

6. MODEL COMPARISON

After demonstrating the good performance of the GC model in flame simulations, let us compare the GC model with other ω_α models for premixed turbulent combustion. An alternative approach to the direct derivation of models for the scalar mixing frequency ω_α is to consider a transport equation for the scalar dissipation rate ε_α. The relation between ε_α and ω_α is given by $\omega_\alpha = \varepsilon_\alpha / \overline{\phi_\alpha''^2}$. The structure of scalar dissipation rate models can be illustrated by the model of Mura and Borghi [15], which is applicable to premixed turbulent combustion. The latter model is given by

$$\frac{\partial \langle\rho\rangle \varepsilon_\alpha^{MB}}{\partial t} + \frac{\partial \langle\rho\rangle (\overline{u}_k - \overline{U}_{L_k})\varepsilon_\alpha^{MB}}{\partial x_k} = \frac{\partial}{\partial x_k}\left(\langle\rho\rangle D_t \frac{\partial \varepsilon_\alpha^{MB}}{\partial x_k}\right) + c_\alpha \langle\rho\rangle \frac{\varepsilon}{k} P_\alpha' + \left(c_U \frac{\varepsilon}{k}\frac{P}{\varepsilon} + \alpha\frac{\varepsilon}{k} - \beta' \frac{\varepsilon_\alpha^{MB}}{\overline{\phi_\alpha''^2}}\right)\langle\rho\rangle \varepsilon_\alpha^{MB}. \quad (7)$$

The model (7) was derived on the basis of flamelet assumptions for infinitely high Damköhler numbers. The source terms on the right-hand side are related to the production and dissipation terms that appear in transport equations for the turbulent kinetic energy and scalar variances. The propagation term $\overline{U}_{L_k}$ of flamelets and the parameter β' are functions of the laminar burning velocity, scalar gradients and the turbulent kinetic energy [15]. The model constants are

given by $\alpha = 0.9$, $\beta = 4.2$, $c_U = c_\alpha = 1.0$, $c_{\varepsilon_\alpha} = 0.1$ and $Sc_{\varepsilon_\alpha} = 1.3$. The model (7) will be referred to below as Mura and Borghi (MB) model. As an alternative to the MB model, Lindstedt and Vaos [5] derived an expression for ω_α which is given by

$$\omega_\alpha^{LV} = \frac{C_\alpha^{'}}{2}\left(1 + C_\alpha^{*}\frac{\rho_u}{\langle\rho\rangle}\frac{S_L}{v_k}\right)\frac{\varepsilon}{k}. \qquad (8)$$

Here, $C_\alpha^{'} = 4$ and $C_\alpha^{*} = 1.2$ are model constants [5]. ρ_u denotes the density of the unburned mixture, $\langle\rho\rangle$ is the mean mass density, and v_k is the Kolmogorov velocity. The essential assumption related to the Lindstedt and Vaos (LV) model (8) is given by the consideration of $C_\alpha^{'}$ as a constant, which corresponds to the idea of a local equilibrium between production and dissipation in the scalar frequency transport equation. The simplest ω_α model is recovered by neglecting chemistry effects in the LV model,

$$\omega_\alpha^{ST} = \frac{C_\alpha}{2}\frac{\varepsilon}{k}. \qquad (9)$$

The model (9) will be referred to below as standard (ST-*) scalar mixing frequency model, where * refers to the constant value of C_α applied. The basic assumption related to the model (9) is that the scalar mixing frequency ω_α is controlled by the mixing frequency $\omega = \varepsilon/k = 1/\tau$ of large-scale turbulent motions.

To see the differences to predictions based on the GC model, simulations of the F3, F2, and F1 flames have been performed by adopting the MB model, the LV model, and the ST-6 model (in accord with the observations of Lindstedt and Vaos [5] it was found that the combination of the ST-* model with $C_\alpha = 6$ represents an optimal choice). It turned out that the MB model combined with $\beta = 4.2$ did not allow calculations of stably burning F3, F2, and F1 flames. Thus, the MB model was used in conjunction with $\beta = 0.3$, which provided the best agreement between simulation results and measurements. Results obtained with the different frequency models are compared with experimental data in figure 6. This figure shows the mean flame front position which is defined as iso-line of the mean temperature. The iso-line temperatures are $\overline{T}_1 = 1300K$ for the F1 flame, $\overline{T}_2 = 1400K$ for the F2 flame, and $\overline{T}_3 = 1500K$ for the F3 flame respectively. The mean flame front position predicted by the GC frequency model agrees well with the measured positions for all three flames. Thus, the GC frequency model provides very good predictions for a range of combustion regimes. The use of the MB model, LV

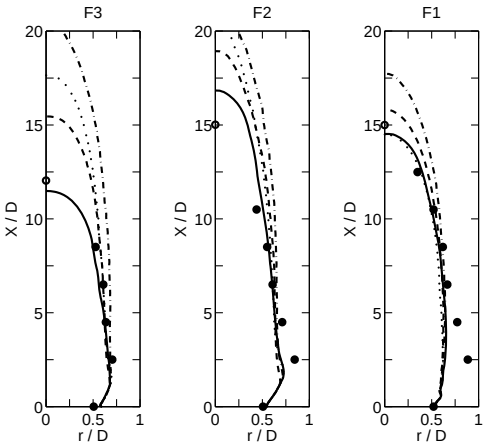

Figure 6: Position of the mean turbulent flame front obtained in F3, F2, and F1 flame simulations by different scalar mixing frequency models: GC model (solid line), MB model (dotted line), LV model (dashed line), ST-6 model (dashed-dotted line). Dots denote experimental results. The circles denote curve fit results to the measured values [8]. The iso-line temperatures are $\overline{T}_1 = 1300K$ for F1 flame, $\overline{T}_2 = 1400K$ for F2 flame, and $\overline{T}_3 = 1500K$ for F3 flame respectively.

model and ST-6 model results in significant overestimations of the axial position of the flame tip regarding the F3 and F2 flames. In the flame tip, the turbulent burning velocity has to balance the high axial velocity of the jet. Thus, predictions of the axial position of the flame tip are very sensitive to an accurate prediction of the turbulent burning velocity. In the F3 and F2 flames, which are close to the flamelet regime, one finds strong axial gradients of mean scalars and scalar variances in the flame tip. These gradients increase the scalar mixing frequency (i.e., the mixing efficiency), which leads to an increase of the turbulent burning velocity. The GC frequency model includes the effects of the strong gradients of scalar means and variances in the flame tip such that the GC model provides an accurate prediction of the flame tip position. In contrast to that, the ST-6 model and the LV model do not include any effects of mean scalar and scalar variance gradients on the scalar mixing. These models underestimate, therefore, the turbulent burning velocity, which explains the overestimation of the flame tip position. The overprediction of the flame tip position observed in the MB model simulations probably results from an underestimation of the chemical reaction contributions [6]. Regarding the mean flame front position

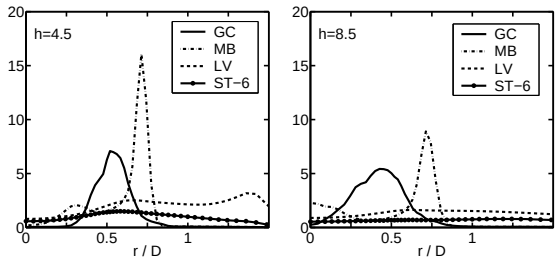

Figure 7: Radial profiles of the normalized scalar mixing frequency $\omega_\alpha \tau_c$ obtained in F3 flame simulations by the GC model (solid line), the MB model (dashed line), the LV model (dashed-dotted line) and the ST-6 model (dotted line). The frequency values have been normalized by the chemical time scale $\tau_c = 0.44\,ms$.

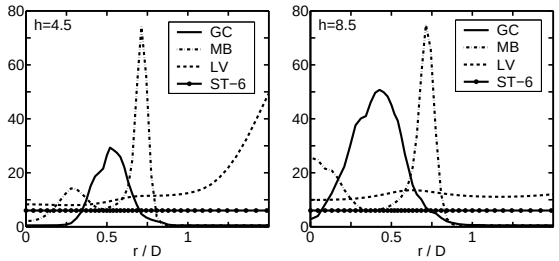

Figure 8: Radial profiles of the mixing coefficient C_α obtained in F3 flame simulations by the GC model (solid line), the MB model (dashed line), the LV model (dashed-dotted line) and the ST-6 model (dotted line).

in F1 flame simulations one finds (with the exception of the ST-6 model) that the predictions of the different mixing frequency models agree well with the measurements. The F1 flame is closer to the well-stirred combustion regime such that the scalar gradients are not as strong as in the F3 and F2 flames. The mixing enhancement is less intense, which explains the close agreement of results.

Figure 7 shows normalized mixing frequencies in F3 flame simulations according to the four scalar frequency models considered. Figure 8 shows the corresponding values of the mixing coefficient C_α. The GC model and the MB model display a peak of the scalar mixing frequency. At both axial positions the peak predicted by the MB model is located further outward than the peak predicted by the GC model. How can this observation explain the different results for the mean flame front position? In an analogy to a 1-d laminar flame the turbulent flame brush can be divided into a preheat zone (fresh gas side of the flame front) and a reaction zone (burnt gas side of the flame front). The peak value of the scalar mixing frequency predicted by the GC model is then located in the preheat zone and the peak predicted by the MB model is located in the reaction zone of the turbulent flame brush. The preheat zone is the zone where the temperature of the fresh mixture is increased due to convection and diffusion of heat from the reaction zone where most of the chemical reactions and the heat release take place. High values of the scalar mixing frequency in the preheat zone allow for a faster mixing of the temperature and thereby reactions can take place at further inward radial locations. Without enhanced mixing in the preheat zone the location of the reaction zone will be located further outward. Due to the heat release the location of the reaction zone determines the mean flame front position. Therefore, one would expect that the mean flame front position predicted by the GC model is located further inward than the position predicted by the MB model. Exactly this feature can be seen in figure 6. The scalar mixing frequencies obtained with the ST-6 model and the LV model differ significantly from the values predicted by the GC model and the MB model: these scalar mixing frequency profiles are rather flat, and they do hardly show a peak. The latter behavior results from the fact that both models do not account for mean scalar and scalar variance gradients.

7. SUMMARY

Previously developed PDF methods for premixed turbulent combustion were considered in detail in section 6. This discussion revealed significant problems of existing approaches to model the scalar mixing frequency. The GC frequency model was introduced here as an alternative to these existing PDF methods for premixed turbulent combustion. The modeling concept applied is relatively general: the GC model is constructed such that deviations of a local equilibrium between production processes and dissipation of scalar variances become minimal. This concept offers significant conceptual advantages compared to existing methods. Empirical parametrizations are not involved, there is no need to adjust several model parameters to the flow considered, and effects of chemical reactions on scalar mixing frequencies are involved without making assumptions that have an uncertain range of applicability.

The suitability of the GC scalar frequency model was demonstrated by applications to several turbulent premixed Bunsen flames that cover various regimes rang-

ing from flamelet to distributed combustion. Comparisons with existing scalar mixing frequency models for premixed turbulent combustion revealed the advantages of the GC frequency model.

Many real flames involve a variety of mixing regimes (non-premixed, partially-premixed and premixed turbulent combustion). A significant advantage of the approach presented here is given by its applicability to such flames involving several combustion regimes. Obviously, such applications will be very valuable for the further evaluation of the capabilities of the approach presented. Questions that need further investigations concern, for example, the relevance of using more complex scalar mixing models and the relevance of using specific scalar mixing frequencies for different species. It is worth noting that essentially the same modeling approach can be used within the framework of scalar filter density function (FDF) methods.

ACKNOWLEDGEMENTS

This work has been supported by the German Research Foundation (DFG) and Fluent Inc. (DFG Transfer Project 42). In particular, we are very thankful to Dr. M. Braun (Fluent Germany) and Professor R. Friedrich for significant support regarding the realization of this project. The authors gratefully acknowledge valuable support of Dr. G. Goldin (Fluent USA) regarding the realization of computations. We are very thankful to Professor P. Jenny for many helpful comments on our work. The computational resources have been provided by the Institute of Scientific Computation (ISC) at the University of Wyoming.

REFERENCES

[1] S. Heinz. *Statistical Mechanics of Turbulent Flows*. Springer-Verlag, Berlin, 2003.

[2] R.O. Fox. *Computational Models for Turbulent Reacting Flows*. Cambridge University Press, Cambridge, UK, 2003.

[3] M.S. Anand and S.B. Pope. Calculations of premixed turbulent flames by PDF methods. *Combustion and Flame*, 67(2):127–142, 1987.

[4] A. Mura, F. Galzin, and R. Borghi. A unified PDF-flamelet model for turbulent premixed combustion. *Combustion Science and Technology*, 175(9):1573–1609, 2003.

[5] R.P Lindstedt and E.M. Vaos. Transported PDF modeling of high-Reynolds-number premixed turbulent flames. *Combustion and Flame*, 145(3):495–511, 2006.

[6] M. K. Stöllinger and S. Heinz. PDF modeling and simulation of premixed turbulent combustion. Submitted for publication, 2008.

[7] C. Dopazo and E.E. O'Brien. An approach to autoignition of a turbulent mixture. *Acta Astronautica*, 1(9-10):1239–1266, 1974.

[8] Y.C Chen, N. Peters, G.A. Schneemann, N. Wruck, U. Renz, and M.S. Mansour. The detailed flame structure of highly stretched turbulent premixed methane-air flames. *Combustion and Flame*, 107(3):223–244, 1996.

[9] T. H. Shih, W. W. Liou, A. Shabbir, Z. Yang, and J. Zhu. A new $k-\varepsilon$ eddy-viscosity model for high Reynolds number turbulent flows - model development and validation. *Computers and Fluids*, 24(3):227–238, 1995.

[10] R.R. Cao and S.B. Pope. Numerical integration of stochastic differential equations: Weak second-order mid-point scheme for application in the composition PDF method. *Journal of Computational Physics*, 185(1):194–212, 2003.

[11] FLUENT. *6.3 User Guide*. FLUENT INC., Lebanon, NH, 2006.

[12] A. Kazakov and M. Frenklach. *DRM22*. www.me.berkeley.edu/drm/.

[13] S.B. Pope. Computationally efficient implementation of combustion chemistry using a *in situ* adaptive tabulation. *Combustion Theory and Modelling*, 1(1):41–63, 1997.

[14] H. Pitsch and L.D. De Lageneste. Large eddy simulation of premixed turbulent combustion using a level-set approach. *Proceedings of the Combustion Institute*, 29:2001–2008, 2002.

[15] A. Mura and R. Borghi. Towards an extended scalar dissipation equation for turbulent premixed combustion. *Combustion and Flame*, 133 (1-2):193–196, 2003.